Supplementary Materials

Design of Two-Dimensional Organic-Inorganic Heterostructures for High-Performance Electromagnetic Wave Absorption

Jun Chen [a], Weiping Ye [a], Shuai Wang [a], Kunyao Cao [a], Yue Zhang [a], Jiayue Wen [a], Rui Zhao [a*] and Weidong Xue [a*]

a School of Materials and Energy, University of Electronic Science and Technology of China, Chengdu 610054, China
* Rui Zhao, ruizhao@uestc.edu.cn; Weidong Xue, xuewd@uestc.edu.cn

2. Experiment Section

2.1. Preparation of Polythiophene Intercalated V_2O_5 Composite PTVOs

PTVO composite was prepared by a simple hydrothermal process. First, 1 mmol NH_4VO_3 and 30 μL thiophene solution were added to 21 mL of deionized water and stirred for 15 minutes. Then, 1 mol/L of HCl was added in the continuous agitation, the pH value of the solution was adjusted to 1, and the agitation continued for 15 minutes. Finally, the solution was transferred to a 60ml Teflon-lined stainless-steel autoclave and reacted at 120°C for 24 hours. The product PTVO-30 was collected by centrifugation and then washed several times with ethanol and deionized water. Finally, the product was frozen at minus 30 degrees Celsius for 6 hours and then dried in a freeze-dryer for 24 hours. Polymer-free V_2O_5 was synthesized by the same method without the addition of pyrrole. In addition, different amounts of thiophene solution (5 and 60 μL) were used to prepare polythiophene interlayered V_2O_5 composites, named PTVO-5 and PTVO-60.

2.2. Preparation of Polyaniline Intercalated V_2O_5 Composite PAVOs and Polypyrrole Intercalated V_2O_5 Composite PPVOs

Polyaniline intercalated V_2O_5 composite PAVOs and polypyrrole intercalated V_2O_5 composite PPVOs were synthesized by the same method as PTVOs.In addition, different quantities of aniline solution (5,30 and 60 μL) were used to prepare polyaniline intercalated V_2O_5 composites, named PAVO-5,PAVO-30 and PAVO-60. Different amounts of pyrrole solution (5,30 and 60 μL) were used to prepare polypyrrole intercalated V_2O_5 composites, named PPVO-5,PPVO-30 and PPVO-60.

2.3. Characterization

The structures and morphologies of V_2O_5,PTVOs,PAVOs and PPVOs were characterized by scanning electron microscopy (SEM, Phenom ProX) and transmission electron microscopy (TEM, JEM-2100F). X-ray diffraction (XRD) patterns were

obtained using Cu Kα radiation (λ = 0.15406 nm) on a MiniFlex 600 (Rigaku) X-ray diffractometer. The electronic states of PTVO-30 was analyzed with the help of XPS (Thermo SCIENTIFICK-Alpha). Fourier transform infrared (FTIR) spectra were obtained using Thermo Fisher Nicolet Is10. The electromagnetic parameters of the samples were measured by using vector network analyzer (Keysight E5063A) in the frequency range of 2-18 GHz and using coaxial test fixture. Sample material powder and paraffin blocks were mixed at a ratio of 4:6 and heated. And the mixture was moulded into a cylindrical rings with an inner diameter of 3.04 mm and an outer diameter of 7.0 mm.

2.4 Finite Element Simulation

Taking PTVO-30 composites as an example, simulations were performed in COMSOL software using the RF module, and corresponding models were built to investigate the ability of electromagnetic energy loss in organic-inorganic heterostructured composites with nanoflower morphology.The solution model can be divided into three layers, namely the upper and lower perfect match layers and the intermediate study object layer. The perfect match layer is used to absorb the reflected and transmitted electromagnetic waves. The study object has paraffin wax as the substrate and PTVO-30 composite as the absorbing material. The electromagnetic wave with a power of 1 W (frequency of 12.48 GHz) is emitted from the source port and induced into the MA material along the Z-axis, with the electric field direction in the X-axis. In addition, the established models are divided into a rectangular model for the epoxy resin base and a nanoflower model for the PTVO-30 composite base. The length-width-height dimensions of the rectangular model are both 20 μm. the length-width-height dimensions of the petals of the nanoflower model are 3.0 μm, 0.8 μm, and 0.1 μm, respectively. the diameter of the central sphere is 1.0 μm.

2.5. RCS Simulation

The calculations were performed using the Rader Cross Section under the microwave&RF/OPTICAL module in CST. According to the single-layer uniform

absorber model, for the three research objects PTVO-30,PAVO-30 and PPVO-5, the absorbent layer with the thickness of 2.1 mm, 1.7 mm and 2.0 mm and the ideal metal conductor backplane with the thickness of 2.0 mm are respectively adopted. The length and width of the two layers are 300 mm * 300 mm respectively. The electromagnetic parameters of the absorber are measured by a vector network analyzer. The measured electromagnetic parameters are imported into CST, and the electromagnetic parameters of the absorber are obtained by fitting with the dispersion model. Open (add space) boundary conditions are set in all directions. The field monitor type is RCS. The linear polarized plane wave is used, and the electric polarization propagation direction is along the X-axis. The RCS values can be calculated by using the equation,

$$\sigma(dBm^2) = 10log\left[\frac{4\pi S}{\lambda^2}\left|\frac{E_S}{E_i}\right|^2\right] \#(S1)$$

where, S is the area of the target object simulation model, λ is the wavelength of the electromagnetic wave, E_s is the electric field intensity of transmitting waves, and E_i is the electric field intensity of receiving waves.
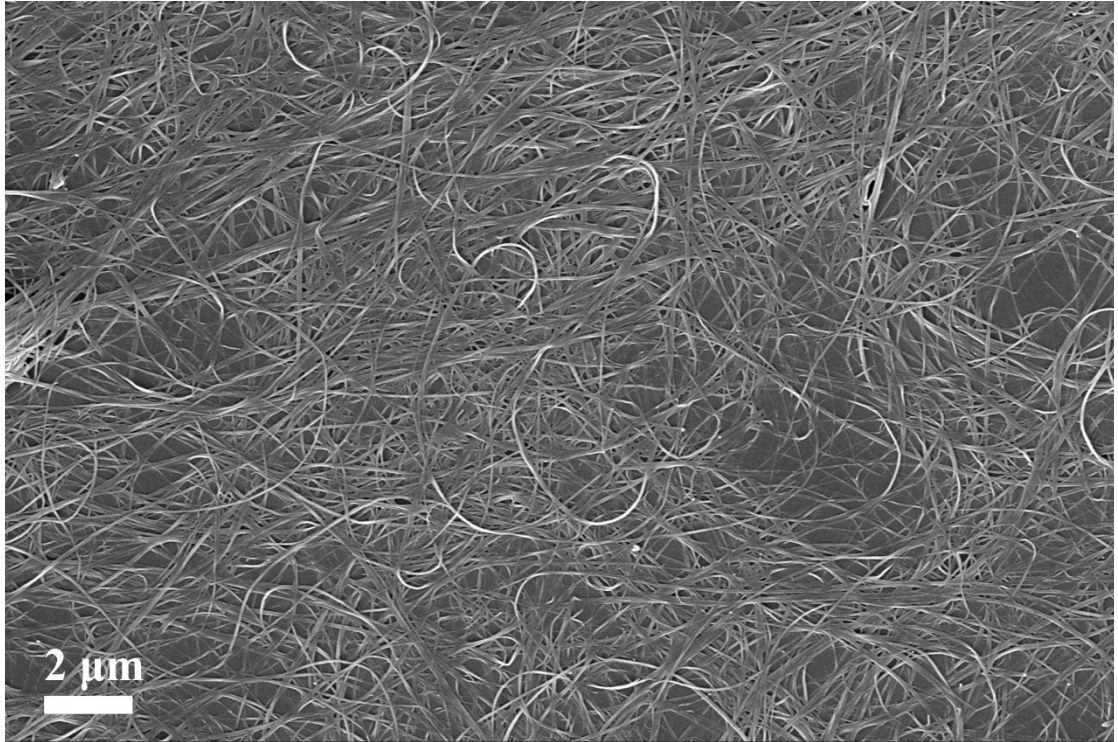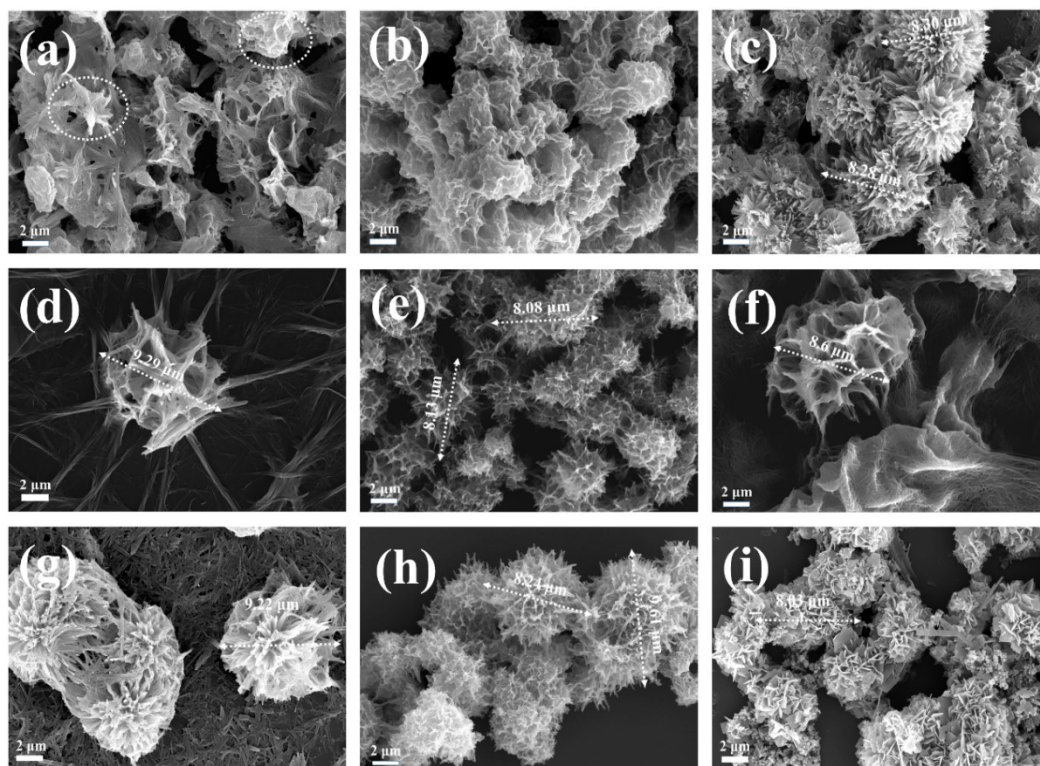

Fig. S1. SEM images of V_2O_5 sample

Fig. S2. SEM images of (a) PTVO-5, (b) PAVO-5, (c) PPVO-5, (d) PTVO-30, (e) PAVO-30, (f) PPVO-30, (g) PTVO-60, (h) PAVO-60, (i) PPVO-60
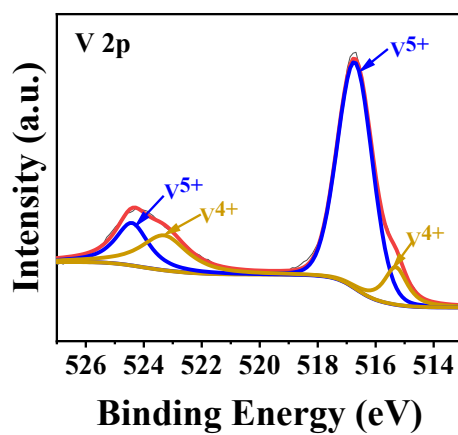

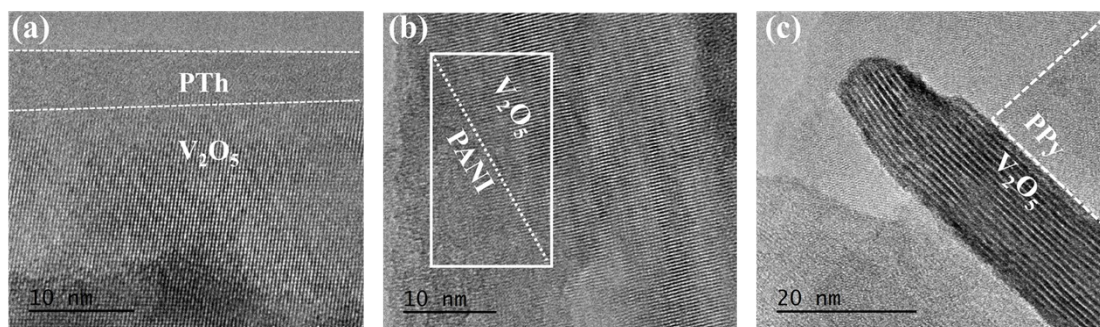**Fig. S3.** XPS spectrum of V 2p of PTVO-30.

Fig. S4. HR-TEM images of (d) PTVO-30, (e) PAVO-30 and (f) PPVO-30.
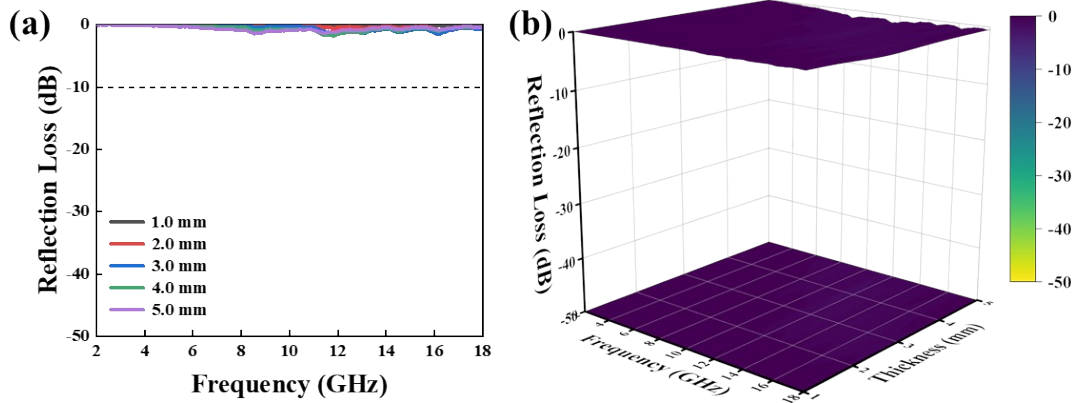
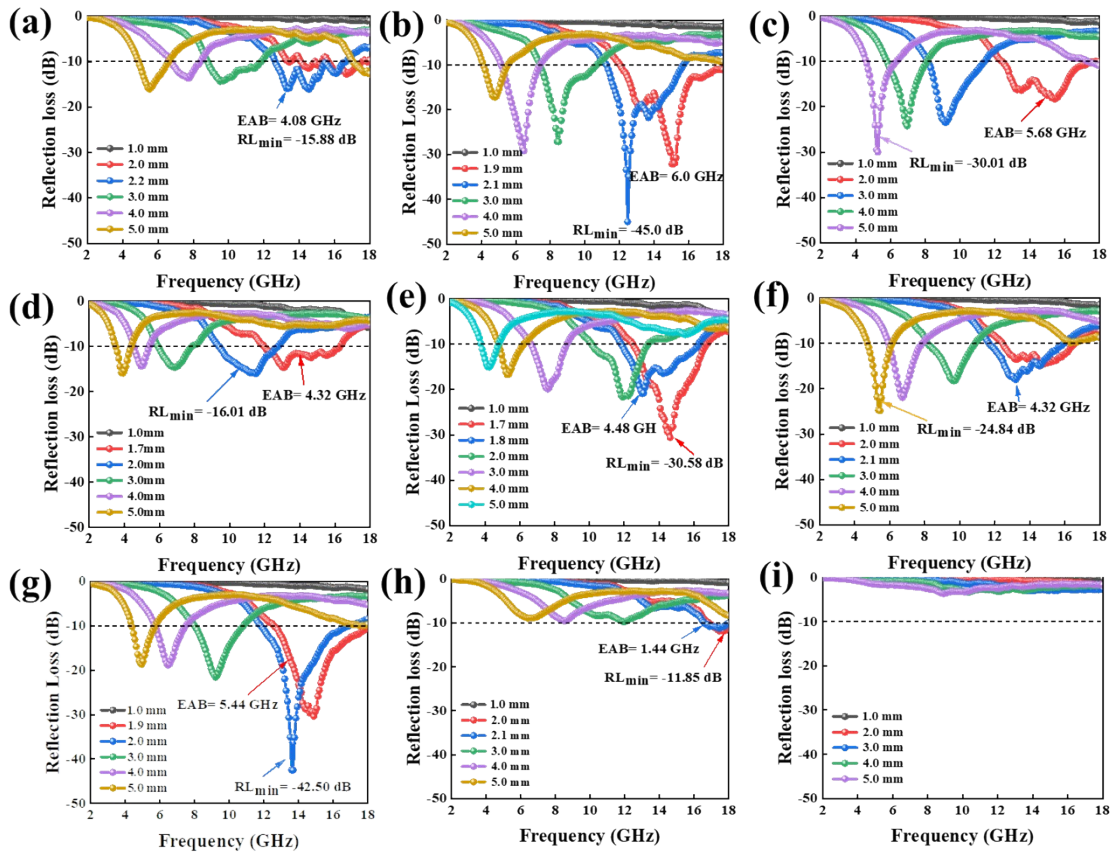**Fig. S5.** (a) 2D and (b) 3D plots of V_2O_5 reflection loss

Fig. S6. 2D plots of reflection loss of conductive polymer interlayer V_2O_5 series. (a) PTVO-5, (b) PTVO-30, (c) PTVO-60, (d) PAVO-5, (e) PAVO-30, (f) PAVO-60, (g) PPVO-5, (h) PPVO-30, (i) PPVO-60
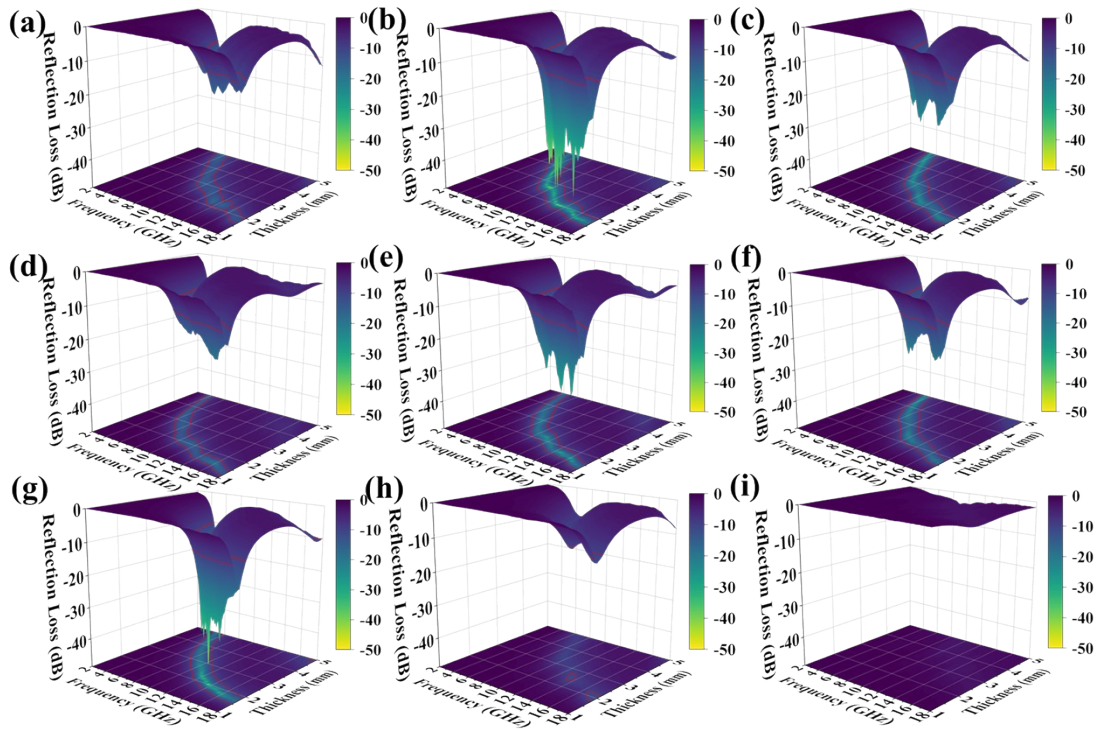
Fig. S7. 3D plots of reflection loss of conductive polymer interlayer V_2O_5 series. (a) PTVO-5, (b) PTVO-30, (c) PTVO-60, (d) PAVO-5, (e) PAVO-30, (f) PAVO-60, (g) PPVO-5, (h) PPVO-30, (i) PPVO-60

Table S1. Comparison of the wave absorption performances of PPV0-5,PAVO-30 and PTVO-30 with recently reported vanadium-based or conductive polymer MA materials.

MAMs	Ratio (wt%)	RL_{min} (dB)	EAB (GHz)	Refs.
V oxide@C	50%	-19.50	5.20	[1]
$VO_2(M)$	20%	-45.80	3.37	[2]
$Co/C@V_2O_3$	50%	-40.10	4.64	[3]
$Fe_3O_4/PPy/CNT$	20%	-25.90	4.50	[4]
PPy/EG	10%	-48.0	3.40	[5]
CoS@PPy	20%	-41.80	5.40	[6]
$rGO/f-Fe_3O_4(1:10)@PANI$	40%	-46.49	4.25	[7]
CFHMP/PTh	73%	-33.80	3.10	[8]

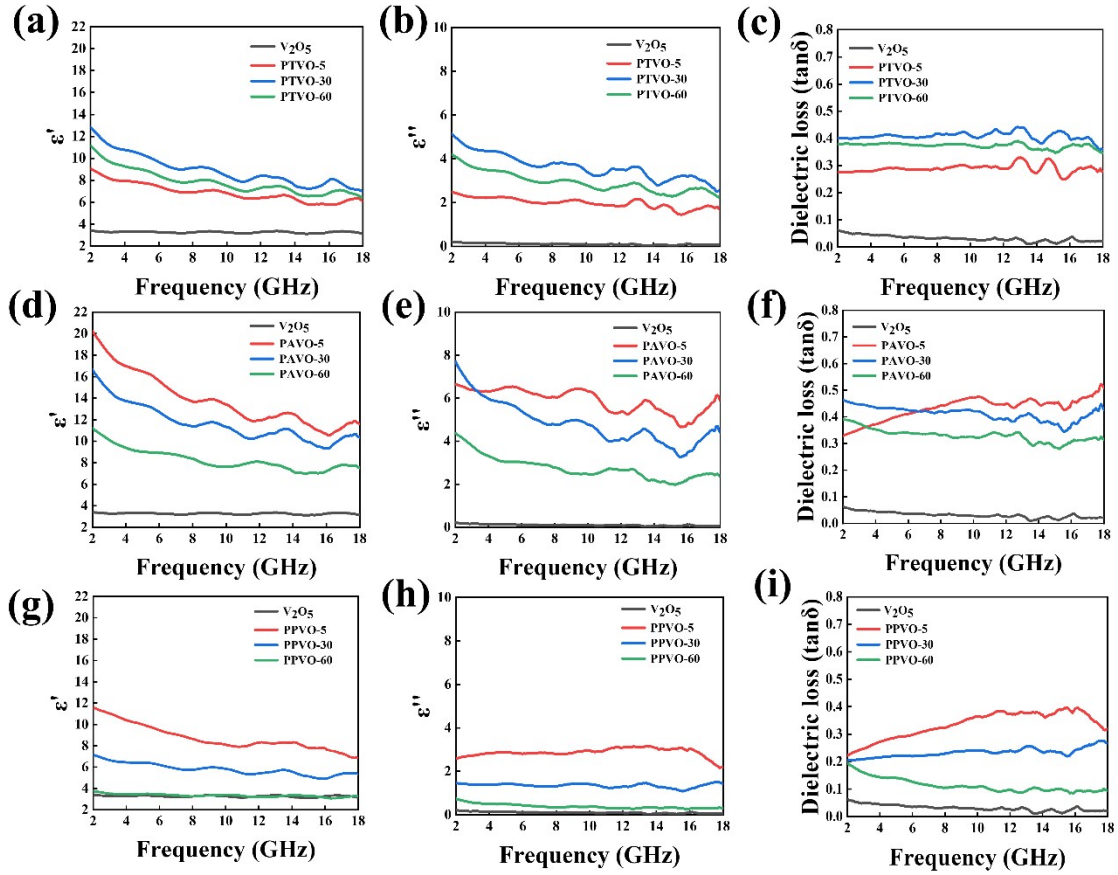|				
Polythiophene/RGO/Fe$_3$O$_4$	50%	-30.20	1.10	[9]
PTVO-30	40%	-45.0	6.0	This work
PAVO-30	40%	-30.58	4.48	This work
PPVO-5	40%	-42.50	5.44	This work

Fig. S8. Frequency-dependent value curves of (a) the real part of the dielectric constant (ε') and (b) the imaginary part of the dielectric constant (ε'') of PTVOs. (c) Frequency-dependent dielectric loss tangents of PTVOs. Frequency-dependent value curves of (d) the real part of dielectric constants (ε') and (e) imaginary part of dielectric constants (ε'') of PAVOs. (f) Frequency-dependent dielectric loss tangents of PAVOs. (g) Frequency-dependent value curves of (g) the real part of the dielectric constant (ε') and (h) the imaginary part of the dielectric constant (ε'') of PPVOs. (i) Frequency-dependent dielectric loss tangents of PPVOs.
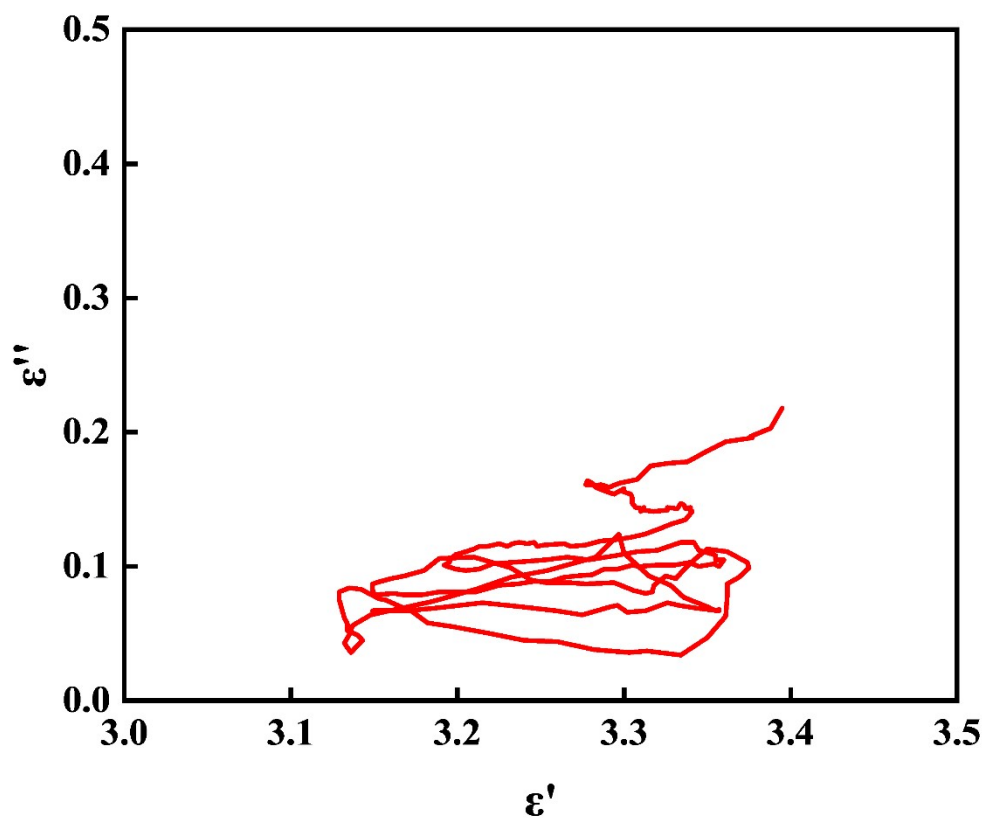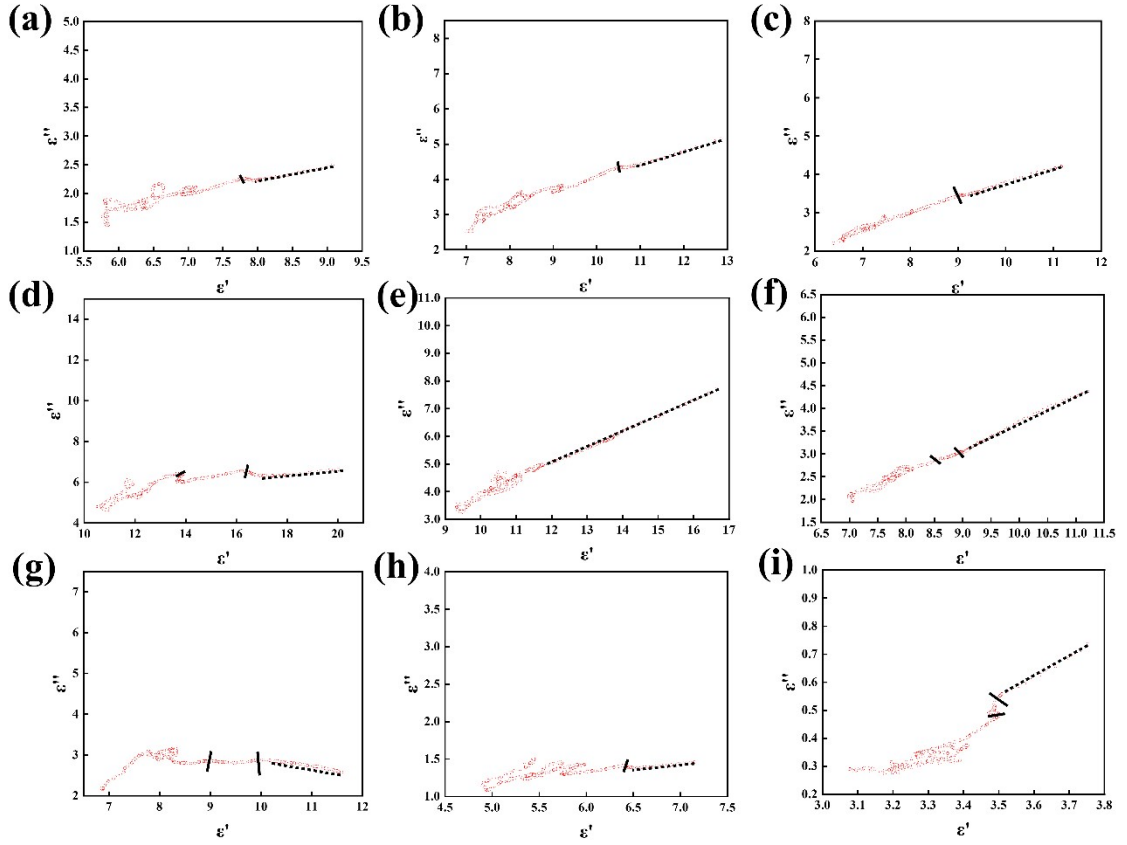
Fig. S9. Cole-Cole curve of V_2O_5

Fig. S10. Cole-Cole curves of (a) PTVO-5, (b) PTVO-30, (c) PTVO-60, (d) PAVO-5, (e) PAVO-30, (f) PAVO-60, (g) PPVO-5, (h) PPV0-30 and (i) PPVO-60
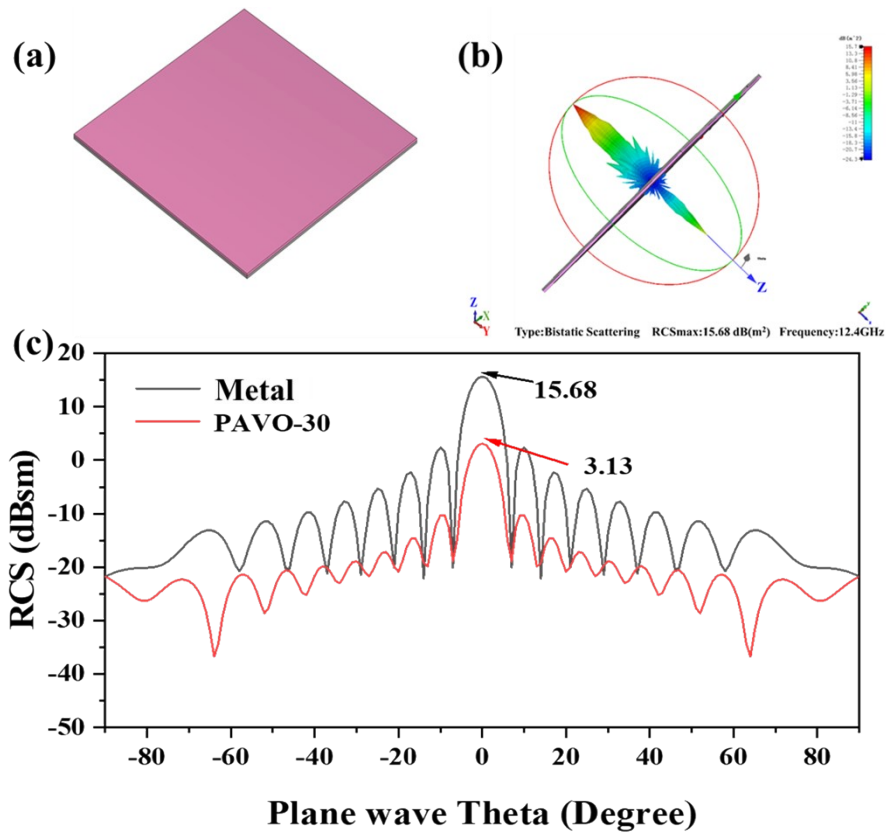
Fig. S11. (a) CST simulation model. (b) Three-dimensional radar wave scattering signal. (c) RCS simulation curves of the ideal metal conductor and PAVO-30 samples at different scanning angles.
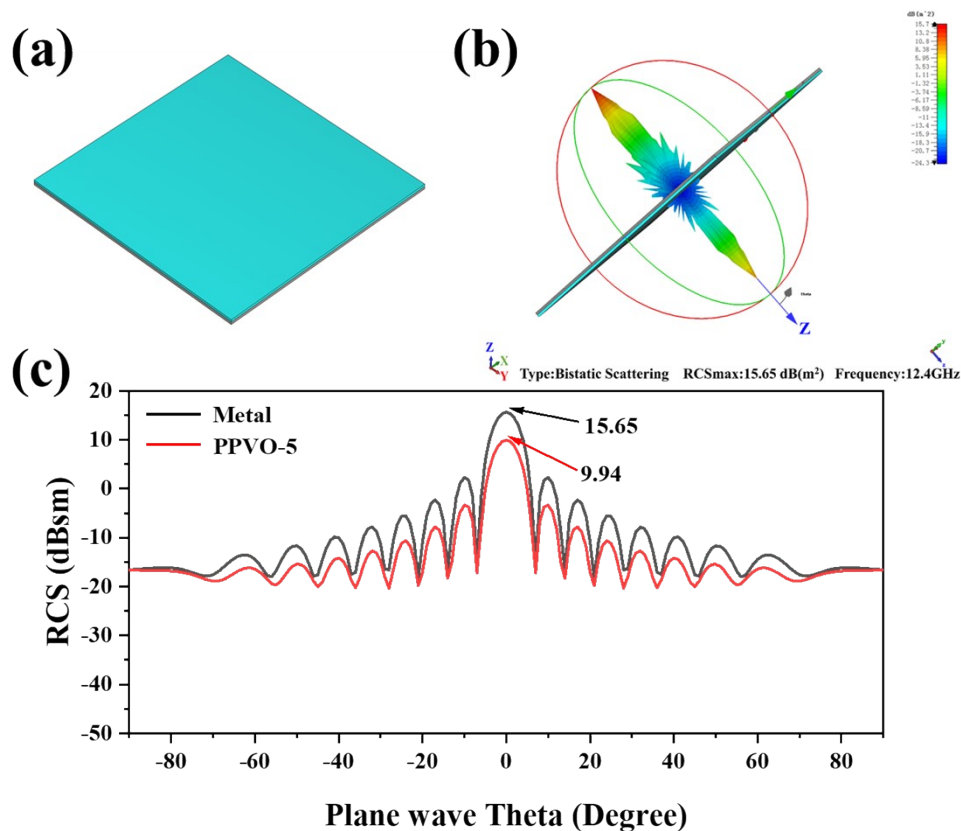
Fig. S12. (a) CST simulation model. (b) Three-dimensional radar wave scattering signal. (c) RCS simulation curves of the ideal metal conductor and PPVO-5 samples at different scanning angles.

References

1   Y. Zhu, X. Guan, Z. Yang and X. Xu, *J. Alloy. Compd.*, 2021, **865**, 158886.
2   Chen, S. Ma, X. Li, X. Zhao, X. Cheng and J. Liu, *J. Alloy. Compd.*, 2019, **791**, 307-315.
3   C. Zhou, C. Wu, D. Liu and M. Yan, *Chemistry - A European Journal*, 2019, **25**, 2234-2241.
4   R. Yang, P. M. Reddy, C. Chang, P. Chen, J. Chen and C. Chang, *Chem. Eng. J.*, 2016, **285**, 497-507.
5   L. Shan, X. Chen, X. Tian, J. Chen, Z. Zhou, M. Jiang, X. Xu and D. Hui, *Composites, Part B*, 2015, **73**, 181-187.
6   H. Liu, G. Cui, L. Li, Z. Zhang, X. Lv and X. Wang, *Nanomaterials*, 2020, **10**, 166.
7   H. Cai, C. Feng, H. Xiao and B. Cheng, *J. Alloy. Compd.*, 2022, **893**, 162227.
8   L. Li, S. Liu and L. Lu, *J. Alloy. Compd.*, 2017, **722**, 158-165.
9   L. Ahmadian-Alam, F. Jahangiri and H. Mahdavi, *Chem. Eng. J.*, 2021, **422**, 130159.